Article

Not peer-reviewed version

Evaluation of Functional Electrospun Chitosan-Based Nanofibers Loaded with Norfloxacin for Enhanced Burn Wound Healing Response

Corneliu-George Coman , Ioannis Gardikiotis * , Carmen Solcan , Cosmin-Gabriel Tartau , Caroline Chabot , Gianina Dodi , Liliana Mititelu Tartau

Posted Date: 17 June 2026

doi: 10.20944/preprints202606.1266.v1

Keywords: electrospun nanofibers; trimethyl chitosan; norfloxacin; wound healing; rat burn model

 doi:10.20944/preprints202606.1266.v1

Article

Evaluation of Functional Electrospun Chitosan-Based Nanofibers Loaded with Norfloxacin for Enhanced Burn Wound Healing Response

Corneliu-George Coman [1,2], Ioannis Gardikiotis [1,3,*], Carmen Solcan [4], Cosmin-Gabriel Tartau [1], Caroline Chabot [5], Gianina Dodi [1] and Liliana Mititelu Tartau [1]

[1] Grigore T. Popa University of Medicine and Pharmacy Iasi, Romania
[2] University of Mons, Faculty of Medicine, Pharmacy and Biomedical Sciences, Department of Surgery, Mons, Belgium
[3] Sfanta Maria Children's Emergency Hospital Iasi, Romania
[4] Ion Ionescu de la Brad University of Life Sciences, Iasi, Romania
[5] Université Catholique de Louvain, Cliniques Universitaires Saint Luc, Department of Radiology, Brussels, Belgium
* Correspondence: dr.gardikiotis@yahoo.com

Abstract

Background: Nanofibrous materials based on chitosan (CS) have attracted considerable attention for advanced wound management due to their favourable biocompatibility, biodegradability, and potential as drug delivery platforms. Additional surface functionalization may improve their interaction with the wound environment and influence tissue repair mechanisms. **Method:** Electrospun trimethyl chitosan (TMC)/CS nanofibers were developed and further processed into three different variants: unloaded fibers (NCC), norfloxacin-encapsulated fibers (NCX), and norfloxacin-loaded fibers functionalized with 2-formylphenylboronic acid (NCXA). The obtained systems were investigated through scanning electron microscopy (SEM), Fourier-transform infrared spectroscopy (FTIR), thermogravimetric analysis (TGA), and UV–Vis spectroscopy. Their therapeutic potential was assessed in vivo using a standardized deep dermal burn model in Wistar rats, with vaseline gauze and silver sulfadiazine employed as reference treatments. Healing progression was monitored through macroscopic evaluation using histopathology, immunohistochemical markers (TNF-α, IL-1β, IL-17, VEGF, VCAM, CD163), and systemic IL-8 determination. **Results:** Physicochemical characterization verified homogeneous nanofiber formation, efficient incorporation of norfloxacin, and successful functionalization of the nanostructures. All electrospun formulations promoted improved healing outcomes relative to the untreated control group. Among them, the norfloxacin-encapsulated fibers formulation demonstrated the best healing effect, characterized by faster re-epithelialization, attenuation of inflammatory mediators during later healing stages, and superior tissue architecture restoration. Conversely, the norfloxacin-loaded fibers functionalized with 2-formylphenylboronic acid system maintained a more persistent inflammatory state and exhibited slower transition into the remodelling phase. **Conclusion:** Trimethyl chitosan-based nanofibers loaded with norfloxacin show strong potential as multifunctional wound dressing platforms capable of controlled drug release. The findings emphasize that formulation composition plays a critical role in regulating inflammation and tissue regeneration, underscoring the need for continued refinement of chitosan-derived nanosystems for burn wound therapy.

Keywords: electrospun nanofibers; trimethyl chitosan; norfloxacin; wound healing; rat burn model

 doi:10.20944/preprints202606.1266.v1

1. Introduction

Burn injuries represent one of the most significant challenges in modern healthcare, affecting millions of individuals worldwide and generating substantial medical and socioeconomic burden. Their management is often complicated by the prolonged healing period, the high risk of infection, and the extensive resources required for continuous wound monitoring and care. In addition to the direct clinical impact, burn treatment involves considerable financial costs related to hospitalization, repeated interventions, specialized therapies, and the daily replacement of wound dressings [1]. The multifactorial nature of burn wound healing, which includes inflammation control, prevention of microbial contamination, pain reduction, and stimulation of tissue regeneration, underlines the necessity for more efficient and patient-friendly therapeutic approaches [2].

Frequent dressing replacement remains one of the most distressing aspects of burn care. These repeated procedures may intensify the initial trauma by causing additional tissue damage and severe discomfort, often requiring repeated administration of general anaesthesia, particularly in patients with extensive injuries [1,2]. Beyond the immediate physical suffering, recurrent painful interventions can also contribute to long-term psychological complications, including anxiety, post-traumatic stress disorder, and persistent chronic pain syndromes. Consequently, improving dressing performance and reducing the frequency of dressing changes have become important objectives in the development of modern burn therapies.

In recent years, bioengineered wound dressings have emerged as promising alternatives to conventional materials due to their ability to create a favourable microenvironment for healing while simultaneously delivering antimicrobial and regenerative agents [3]. Such advanced systems are increasingly investigated as potential next-generation solutions for burn wound management, offering enhanced biocompatibility, improved moisture balance, controlled therapeutic delivery, and reduced patient discomfort [1–3].

An effective wound dressing (schematically presented in Figure 1) should combine multiple functional characteristics that actively support the healing process. Besides providing mechanical protection and creating a controlled barrier against external contaminants [4], modern dressings are expected to maintain an optimal wound microenvironment and adapt dynamically to the changing physiological conditions that occur throughout the different stages of tissue repair [5–8]. Such multifunctional systems are particularly important in burn care, where the healing process is frequently complicated by excessive inflammation, microbial colonization, and impaired tissue regeneration.

Among the biomaterials explored for advanced wound management, chitosan (CS) has gained considerable interest due to its constructive biological and physicochemical properties.

Figure 1. Ideal dressing characteristics.

 doi:10.20944/preprints202606.1266.v1

Derived from chitin, chitosan is a biodegradable and biocompatible polysaccharide known for its intrinsic antibacterial, antiviral, and antifungal activities, as well as its haemostatic capacity and ability to absorb wound exudates. These features make CS especially attractive for the development of burn wound dressings and regenerative biomaterials [3,9–12]. Furthermore, chemically modified water-soluble derivatives of chitosan, such as N,N,N-trimethyl chitosan chloride (TMC), exhibit improved solubility over a broad pH range together with enhanced antimicrobial performance, thereby expanding their biomedical applicability [13–15].

An additional advantage of chitosan-based matrices lies in their ability to incorporate and release therapeutic agents through physical interactions or chemical bonding mechanisms. In this context, norfloxacin, a fluoroquinolone antibiotic, represents a valuable candidate for localized antimicrobial therapy. Although the systemic administration of norfloxacin has become more limited due to concerns regarding adverse effects, its local delivery remains highly beneficial for preventing bacterial infection in wounds. Previous investigations have demonstrated a synergistic antibacterial effect between norfloxacin and chitosan, highlighting the potential of this combination for advanced wound dressing applications [16–19].

Recent progress in nanotechnology and scaffold engineering has further improved the performance of chitosan-derived dressings. In particular, nanostructured systems possessing pH-responsive behaviour and high liquid absorption capacity can interact dynamically with the wound environment, making them suitable for the treatment of ulcerative lesions and moderate-to-severe burns [11,20,21]. Building upon these advances, several studies have focused on the development and characterization of a novel patented chitosan-based dressing with unique structural and functional features [22–26]. In light of these findings, the present study aimed to evaluate the therapeutic effectiveness of a composite CS/TMC dressing in an experimental rat burn model and to further investigate its associated immunohistochemical/biological response profile.

2. Materials and Methods

2.1. Materials

All reagents were obtained from Sigma-Aldrich Chemical Co. (Steinheim, Germany) and utilized without further purification. Chitosan (127 kDa, 97% degree of deacetylation) was synthesized via alkaline hydrolysis of low-molecular-weight chitosan. Other chemicals employed included acetic acid (99.89%), norfloxacin (98%), poly(ethylene oxide) (PEO, 1000 kDa), 2-formylphenylboronic acid (97%), sodium hydroxide (95%), and ethanol (98.89%).

2.2. Preparation and Characterization of Nanofibers

N,N,N-Trimethyl chitosan (TMC) was synthesized according to a previously reported protocol without modification [27]. Briefly, a composite solution of CS/TMC/PEO (7:1:2 mass ratio) in 75% acetic acid was electrospun under controlled conditions: 12 kV applied voltage, 0.4 mL/h flow rate, 10 cm needle-to-collector distance, 0.8 mm needle inner diameter, 800 rpm collector rotation, and 27–28 °C (Inovenso NanoSpinner StarterKit). The resulting nanofiber mats were washed with dry ethanol to remove the sacrificial polymer. Composite nanofibers (NCXA) were then functionalized through a two-step process: (1) norfloxacin loading via equilibrium adsorption by immersion in 0.1% ethanolic solution for 24 h (NCX), and (2) surface imination by spraying with 0.2% ethanolic solution of 2-formylphenylboronic acid. The aldehyde content was adjusted to achieve a 10:1 molar ratio of glucosamine to aldehyde units [28].

Dual CS/TMC nanofibers were fabricated using PEO as a sacrificial agent, subsequently removed by ethanol treatment [29]. Norfloxacin, a broad-spectrum antibiotic, was incorporated via immersion in ethanolic solution, achieving a loading of 3.53 ± 0.95%. The norfloxacin-loaded fibers were then surface-functionalized through reversible imine bonds with 2-formylphenylboronic acid, an antimicrobial agent exhibiting potent antifungal and antioxidant activity [30,31].

 doi:10.20944/preprints202606.1266.v1

Fiber characterization was performed as follows. FTIR spectra were recorded in ATR mode using a VERTEX 70 FT-IR spectrophotometer (Bruker, Karlsruhe, Germany) over 4000–600 cm^{-1}, with 32 scans at 4 cm^{-1} resolution, analyzed via OPUS 6.5 software. Morphology was examined by field emission scanning electron microscopy (SEM, EDAX-Quanta 200, Thermo Fisher Scientific, Waltham, MA, USA) at 20 kV and by polarized optical microscopy (Axio Imager M2, Zeiss, Jena, Germany) under cross-polarized light. Norfloxacin loading was quantified by UV–Vis spectroscopy (Cary 60, Agilent, Santa Clara, CA, USA) at 272 nm using the Lambert-Beer law and a calibration curve. Thermal stability was assessed by thermogravimetric analysis (TGA) using an STA 449 F1 Jupiter analyser (platinum pan, 100 µL) over 30–600 °C at 10 °C/min.

2.3. Animals

Experimental procedures were performed on healthy, non-genetically modified, specific pathogen-free adult male Wistar rats (300–350 g) obtained from the Cantacuzino National Institute for Research and Development (Băneasa Station, Bucharest, Romania). Animals were acclimated for 7 days under controlled environmental conditions: temperature 21 °C ± 2 °C, relative humidity 50±5%, and a 12 h/12 h light/dark cycle. Standardized food pellets and water were provided ad libitum.

The study was carried out at the Grigore T. Popa University of Medicine and Pharmacy Iași at Ostin C. Mungiu Advanced Research and Development Center for Experimental Medicine, with standardized environmental conditions and consistent animal welfare practices throughout the experimental period. The animal study protocol was approved by the Ethical Committee of the university (certificate no. 160/04.03.2022 and Project authorization no. 56/19.02.2022). The study was conducted in strict accordance with applicable national and international ethical guidelines for the care and use of laboratory animals, including the 3R principles of the European Directive 2010/63/EU and Romanian Law No. 43/2014, ensuring the welfare and humane treatment of all animals throughout the study.

2.4. In Vivo Burn Protocol

On Day 0, all animals were anesthetized through isoflurane, weighed, and the hair was shaved on their lateral and dorsal regions. Burns were inflicted using the author's patented original device [36] (Figure 2) by ejecting distilled water vapors at 100 °C (212 °F) on the clean, hair free rat's back skin.

(**a**) (**b**)

Figure 2. (a) Experimental setup for rat preparation. Burn infliction funnel is placed on shaved rat dorsum; **(b)** Burns with tattooed contour and tattooed rat code at the base of the tail. Skin marker used for bony landmarks.

The model generated two burn sites on either side of the dorsal thoracic region, separated by a minimum of 1 cm of intact skin. The protocol, previously validated in earlier studies [37–40], involved a 2-second vapor exposure, which showed to produce consistently deep partial-thickness (Figure 2B) burns [11,39–41]. The burn margins were precisely delineated by tattooing the surrounding intact skin with black inorganic ink using a standard tattoo device.

 doi:10.20944/preprints202606.1266.v1

The animals were divided in 5 groups (5 animals/group) for the 3 types of fibers, namely NCC, NCX and NCXA, 1 for the positive control receiving a thin (≈1 mm) layer of silver sulfadiazine cream (SS) and 1 for the negative control treated with petroleum jelly (V). Each animal had 2 burns on their back, covered with each material, both covered with four circular gauze pads followed by a patented wound dressing device, as explained in the next section. Post-burn analgesia was ensured by intraperitoneal administration of tramadol (20 mg/kg) and continued in the drinking water for a minimum of 3 days [32–35], according to visual rat grimace pain scale.

2.5. Patented Wound Dressing

The patented wound dressing is engineered with a circular base fabricated from 3D-printed PLA, incorporating six banana-shaped piercings designed to facilitate controlled dressing change and a commercially available bi-stable metal lid.

The dressing is completed with a lid featuring a depressible top, enabling precise application and solid retention of therapeutic agents within the dressing chamber [42]. The overall architecture and functional components are depicted in Figure 3, demonstrating the innovative integration of mechanical and biomedical design features.

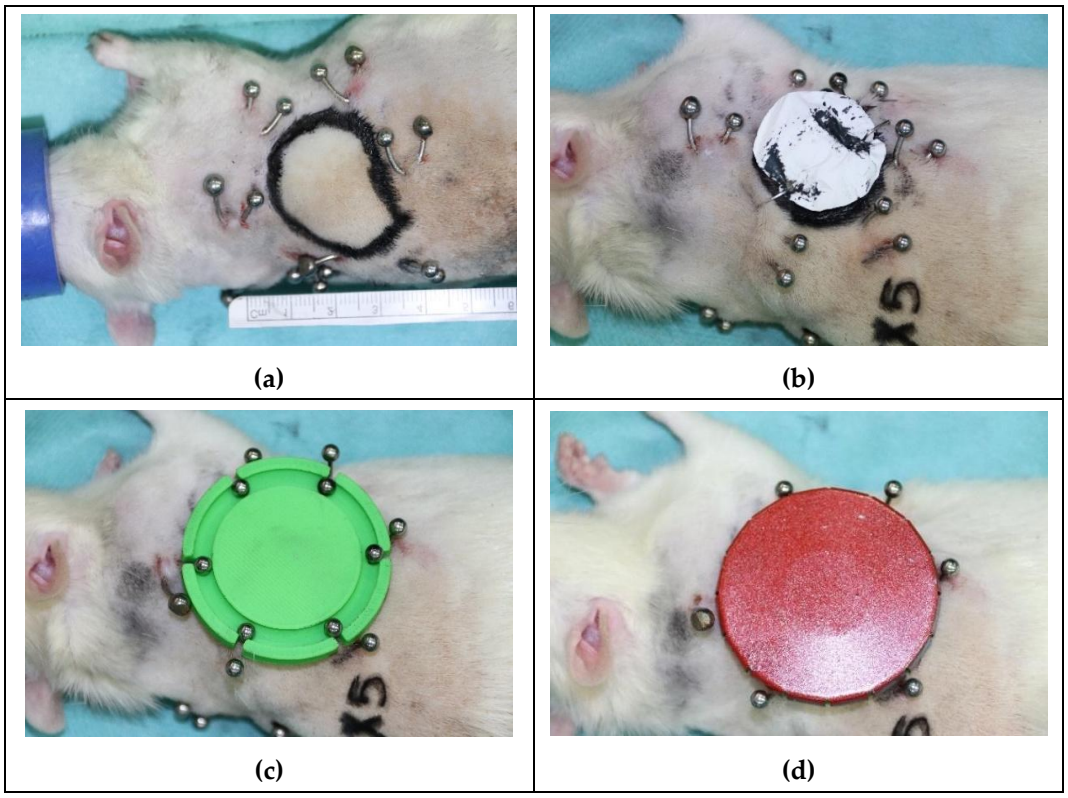

Figure 3. Dressing assembly procedure. **(a)** Piercing placement (60 degrees, equally spaced); **(b)** Chitosan dressing applied; **(c)** Gauze and plastic protection. Piercing balls in their respective slits; **(d)** Ensemble fixation under the metallic bistable lid.

2.6. Follow-Up and Evaluation Protocols

Rats were monitored daily throughout the study, with no significant distress observed. Dressings were applied at day 0 at day 11 only. Digital photographs of the wounds were taken at three time points: immediately after burn induction (day 0), day 11, and day 22. Biopsies were collected on days 11 and 22 under general anaesthesia. Wound areas were quantified by digital planimetry using ImageJ software, and statistical analyses were conducted with SPSS. The study endpoint was defined as complete epithelialization of all wounds within a given group. Euthanasia was performed under general anesthesia via intracardiac injection of 2 mL KCl after the collection of

 doi:10.20944/preprints202606.1266.v1

target organs (liver, kidney, lymph nodes, tendons) and blood samples. All procedures were conducted in accordance with the national and international standards for animal care [32,35,43,44].

The collected tissue samples were embedded in paraffin, sectioned using a microtome, and stained with haematoxylin-eosin (H&E) and immunohistochemically for VEGF, TNF-α, IL-1β, IL-17, VCAM, and CD163 (Bio-Rad Laboratories). Histological examination was performed with an optical microscope equipped with a digital imaging system (Nikon E600 Eclipse) [45–48]. Wound healing was quantified using a modified histological assessment scale [46,49], previously applied in preliminary studies of other chitosan-based formulations [50]. Histological parameters were categorized according to the relevant stages of wound healing: orange for the inflammatory phase (0–7 days), blue for the proliferative phase (3–21 days), and purple for the remodelling phase (2 weeks–1 year). Scores were derived from both H&E and immunohistochemistry slides.

Blood samples collected on days 0 and 22 were used to determine IL-8 concentrations via ELISA, following the manufacturer's instructions (antibodies-online Inc., Aachen, Germany). Briefly, standards and samples (100 µL each) were incubated in the plate for 120 min at 37 °C (Matrix Orbital Delta plus IKA incubator, Staufen, Germany). Detection reagent A (100 µL) was added and incubated for 60 min at 37 °C, followed by three washes. Detection reagent B (100 µL) was then applied, incubated for 30 min, and washed five times. Substrate solution (90 µL) was added, incubated for 30 min, and the reaction terminated with 50 µL stop solution. Absorbance at 450 nm was measured using a Tecan Sunrise microplate reader (Switzerland). Data were analysed using MyAssays online v. R10.2 software (regression analysis with four-parameter logistic) (MyAssays Ltd., Brighton, UK), and IL-8 concentrations were calculated from the standard curve and expressed in pg/mL.

2.7. Statistical Processing of Data

All quantitative data were analysed using SPSS for Windows 17 (IBM Corp., Armonk, NY, USA). Descriptive statistics, including mean ± standard deviation, were calculated for each experimental group. Comparisons between groups were performed using one-way analysis of variance (ANOVA) to assess statistically significant differences. When ANOVA indicated significant differences, post-hoc pairwise comparisons were conducted using Tukey's test to identify specific group differences. A p-value of less than 0.05 was considered statistically significant.

3. Results

3.1. Nanofibers' Characterization

The nanoscale morphology, uniformity, and fiber alignment were characterized using SEM. Representative micrographs are presented in Figure 4, showing a homogeneous distribution of fibers with an average diameter of approximately 160 nm.

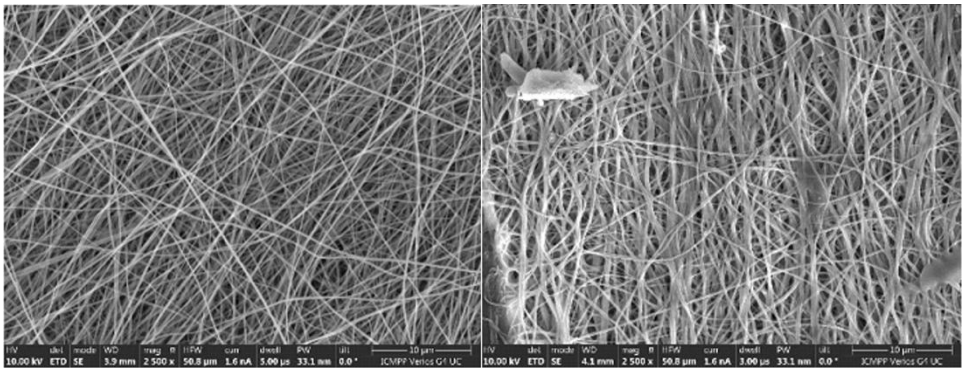

(**a**) (**b**)

 doi:10.20944/preprints202606.1266.v1

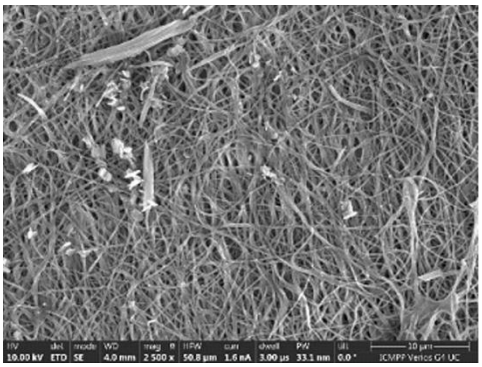

(c)

Figure 4. SEM micrographs of **(a)** blank NCC fibers **(b)** loaded fibers (NCX) and **(c)** further iminated (NCXA).

Thermal stability was assessed by thermogravimetric analysis (TGA, Figure 5a). The initial weight loss corresponded to the evaporation of adsorbed water, while a degradation stage associated with PEO was observed up to 400 °C in pre-treated fibers. This degradation phase was absent in fibers following ethanol-mediated PEO removal, confirming the complete elimination of the sacrificial polymer. Overall, the nanofibers exhibited high thermal resistance under elevated temperatures.

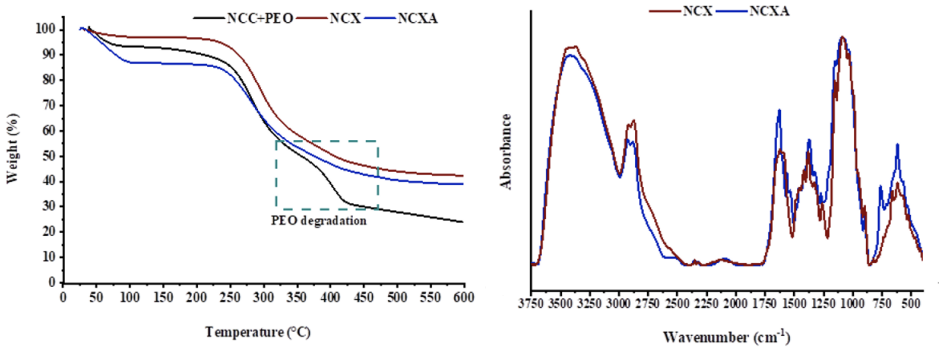

(a) (b)

Figure 5. Representative a. thermograms of NCC fibers containing PEO, and NCX and NCXA composite fibers and b. FTIR comparative spectra of NCX and NCXA fibers revealing the occurrence of imine bonds.

Fiber composition was further verified by FTIR spectroscopy (Figure 5b). The incorporation of norfloxacin was evidenced by characteristic absorption bands, including the NH stretching of the piperazine ring at 1608 cm^{-1}, and the B–O bending vibration indicative of the boronic aldehyde moiety at 842 cm^{-1}. The complete formation of imine linkages was confirmed by the appearance of the C=N stretching band at 1627 cm^{-1}, alongside the disappearance of the carbonyl (C=O) stretching vibration at 1730 cm^{-1} [50,51], demonstrating successful surface functionalization.

3.2. Macroscopical Wound Healing

All animals tolerated the procedures well and demonstrated satisfactory postoperative recovery throughout the study. Progressive wound contraction was observed across all experimental groups, though the rate and extent of healing varied depending on the dressing applied. By day 22, complete epithelialization was achieved in all rats treated with the NCX dressing, indicating its strong wound-healing potential. In contrast, wounds in the V, SS, and NCC groups exhibited near-complete closure, while persistent ulcerations remained in the NCXA group. Analgesic administration was limited to the first five postoperative days, and no unexpected complications were reported, confirming the overall safety and tolerability of all tested interventions.

Quantitative assessment of wound healing revealed that the greatest reduction in wound area was observed in the NCXA group, followed by the V group (T-test, t = 1.09, n – 1 = 19, critical value

 doi:10.20944/preprints202606.1266.v1

= 1.729, p = 0.05). No statistically significant differences were observed between the NCC and NCX groups, while wounds treated with the SS dressing demonstrated the slowest contraction rate. These results suggest that the physicochemical properties and bioactive components of the dressings may have influenced the healing dynamics (Figure 6). For instance, NCX appears to facilitate rapid epithelialization, possibly through enhanced moisture retention and support for cellular migration, whereas the slower healing observed in the SS group may reflect limited bioactivity or suboptimal interaction with the wound microenvironment (Figure 6).

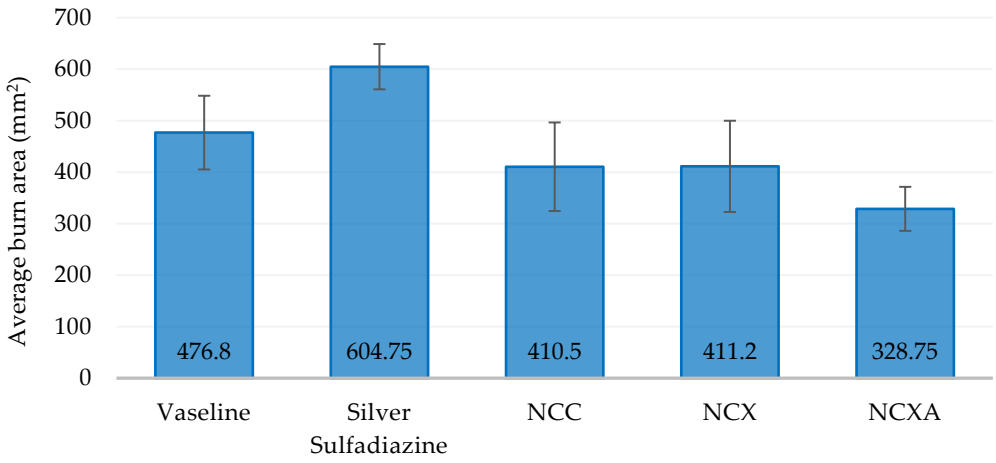

Figure 6. The influence of the dressings used on the burn areas surface at day 22. The values are presented as mean ± standard deviation of mean (S.D.) for 5 rats per group.

At day 0, immediately after burn induction, all experimental wounds exhibited uniform deep dermal damage. In the control animals, the wound was round, slightly depressed, with a whitish appearance, moderate peripheral erythema, and mild oedema. No vesicles or suppuration were observed, and the boundary between the burn area and normal skin was clearly defined. In the nanofiber-treated groups, wounds also had clearly demarcated margins and no signs of infection (Figure 7).

	Day 0	Day 11	Day 22
Vaseline			
Silver sulfadiazine			

 doi:10.20944/preprints202606.1266.v1

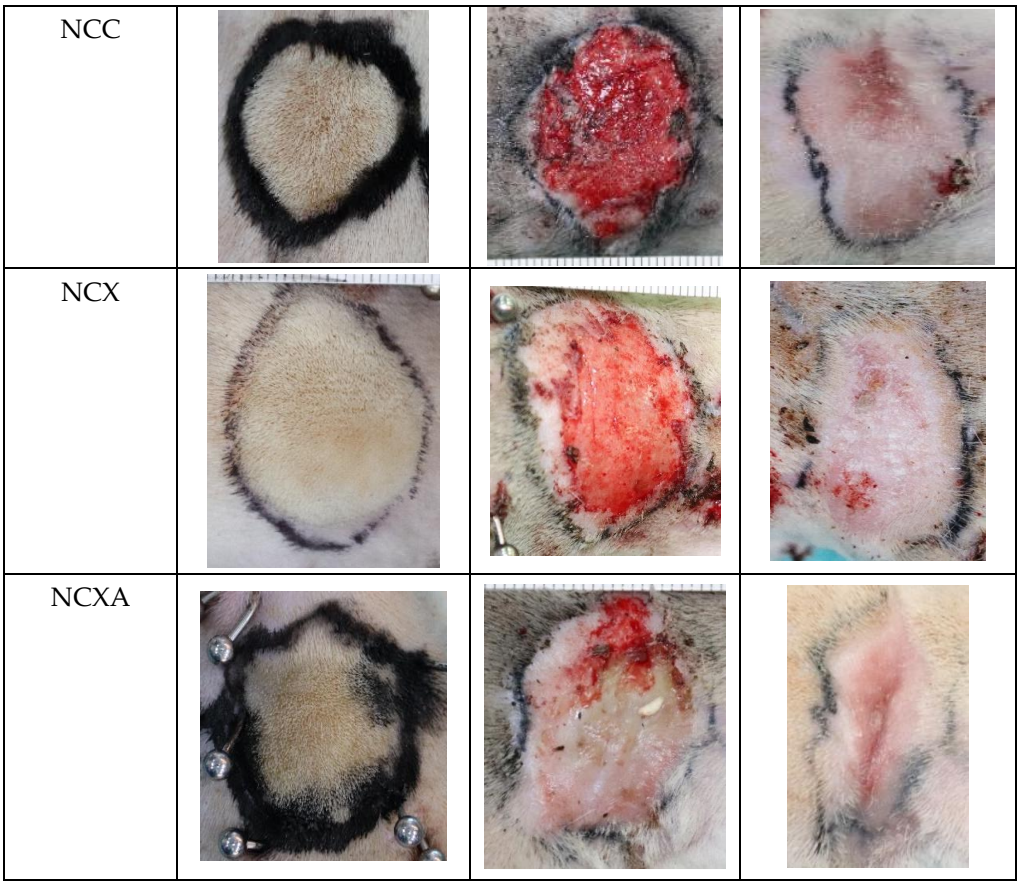

Figure 7. Macroscopical aspect of wound healing evolution in time. Day 0: burn wound with tattooed contour (just outside the burn). Day 11: granulation, centripetal healing. Central fibrin and necrosis in NCXA. Day 22: General good healing rates, although scarring, scabs and ulcerations. Biopsy sites are present in V group.

By day 11, control wounds showed persistent crust formation, slight reduction in wound size, and marginal erythema, but overall healing was slow. In the V, NCC and NCX groups, the burn area exhibited reduced edema, a pinkish coloration, and better-defined borders. Specifically, the NCX-treated wounds displayed early formation of shiny epithelial patches, indicating the onset of tissue regeneration. The NCXA group, however, showed delayed contraction, persistent erythema, and patchy epithelial coverage, suggesting a slower transition from the inflammatory to the proliferative phase (Figure 7).

By day 22, NCX-treated wounds achieved near-complete closure, with smooth tissue and small areas of newly formed epithelium, reflecting advanced regeneration and minimal residual inflammation. NCC-treated wounds showed substantial healing, although minor areas of incomplete epithelial coverage remained. Vaseline-treated wounds retained thick, dark crusts with limited healing, while Silver sulfadiazine-treated wounds displayed moderate closure with partial epithelialization. NCXA-treated wounds exhibited the slowest progress, with persistent irregularities, delayed epithelial coverage, and signs of ongoing inflammation, highlighting a prolonged inflammatory phase and delayed tissue remodelling (Figure 7).

Macroscopic observations indicate that NCX nanofibers promoted the fastest and most organized healing, NCC fibers supported moderate regeneration, while NCXA fibers delayed progression into the remodeling phase, and both control and commercial dressings showed comparatively slower closure, with solely two applications spaced 11 days apart.

The data indicate that the choice of dressing can significantly affect both the rate and quality of burn wound healing, emphasizing the importance of tailoring wound care strategies to the specific properties of the therapeutic material. These findings provide a foundation for further mechanistic studies aimed at optimizing dressing formulations to maximize tissue regeneration and minimize residual ulceration.

 doi:10.20944/preprints202606.1266.v1

3.3. Microscopical Results – Skin Biopsy

3.3.1. Histological Dynamics During Burn Wound Healing

All groups show variable degrees of healing on day 22, as seen in Figure 8. Wounds treated with V, SS, and NCC dressings exhibited partial epithelial restoration. Histological sections revealed areas of continuous epidermis interspersed with immature granulation tissue, moderate inflammatory cell presence, and less organized collagen deposition.

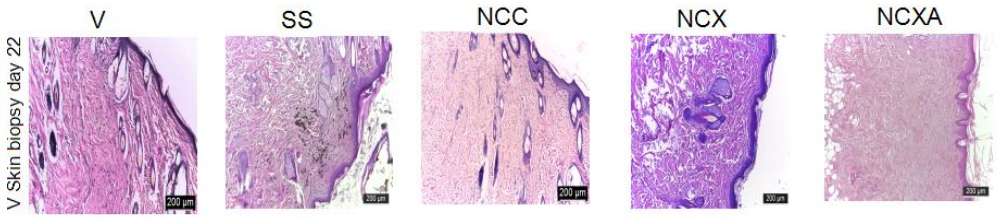

Figure 8. Microscopical wound healing evolution in time. Hematoxylin & Eosin stain x 20. Scale bar = 200 μm.

This pattern aligns with the near-complete wound closure seen macroscopically, reflecting a slightly slower healing trajectory compared to NCX, likely due to less optimal support for cell migration and matrix deposition (Figure 8, Tables 1 and 2). The thickness and regularity of the epithelium is another supporting factor of the skin quality of wounds treated with NCX.

Table 1. Scoring of parameters at day 11; wound score 3: intense; 2: moderate; 1: low; 0: not applicable.

	Wound healing criteria	V	SS	NCC	NCX	NCXA
	Congestion	1	2	1	1	2
	Inflammatory oedema	2	2	2	2	3
	Fibrinous exudate	2	1	1	1	2
	Leucocyte infiltration (neutrophils, macrophage, lymphocyte, histiocyte)	2	2	2	1	2
	Necrosis zone separation and/or resorption	3	2	2	3	2
	Cell differentiation (fibroblasts, endothelial cells)	2	2	2	2	2
	Neoangiogenesis	3	3	3	3	1
	Epithelialization	2	1	1	2	1

Intermediate observations on day 11 revealed pronounced alterations in both the epidermal and dermal layers, following the descending order of severity: V, NCC, NCXA, NCX, and SS. Across all groups, the epidermis exhibited a reduced number of layers (1–3), accompanied by dermal ulcerations infiltrated by macrophages and fibroblasts. As anticipated, tattoo pigments remained fixed immediately outside the burn margins (Figures 7 and 8, Tables 1 and 2). All groups display ongoing neoangiogenesis. Except for NCX, all the other groups display high inflammatory infiltrate and generalized oedema.

Table 2. Scoring of parameters at day 22; wound score 3: intense; 2: moderate; 1: low; 0: not applicable.

	Wound healing criteria	V	SS	NCC	NCX	NCXA
	Congestion	0	0	0	0	0
	Inflammatory oedema	0	0	0	0	1
	Fibrinous exudate	0	1	1	0	2
	Leucocyte infiltration (neutrophils, macrophage, lymphocyte, histiocyte)	2	2	2	1	3
	Necrosis zone separation and/or resorption	1	2	2	1	3

 doi:10.20944/preprints202606.1266.v1

	Cell differentiation (fibroblasts, endothelial cells)	3	3	3	3	2
	Neoangiogenesis	2	2	2	2	3
	Epithelialization	3	3	3	3	2

Histological examination of the burn wounds provided detailed insights into the cellular and tissue-level processes underpinning the healing observed macroscopically. The dermis displayed extensive angiogenesis, with variable degrees of oedema, connective fiber proliferation, and clusters of fibroblasts. Newly formed hair follicles were sparse, small, and thin-walled, interspersed with degenerated follicles (Figures 7 and 8, Tables 1 and 2).

In the NCX-treated group, the histology demonstrated complete re-epithelialization with a well-structured epidermis, organized dermal collagen fibers, and extensive fibroblast proliferation. Inflammatory infiltration was minimal, suggesting resolution of the acute inflammatory phase and efficient progression toward tissue remodelling. These findings are fully consistent with the macroscopic observation of complete epithelial coverage, indicating that NCX supports both rapid and high-quality tissue regeneration (Figure 8, Tables 1 and 2).

The NCXA group, which displayed persistent ulcerations macroscopically, showed histological evidence of incomplete epithelialization, disorganized dermal architecture, sparse fibroblast activity, and ongoing inflammatory infiltration. Collagen fibers were irregular and loosely packed, indicating delayed or impaired tissue regeneration. These cellular-level findings explain the reduced contraction and slower healing observed in this group, highlighting a suboptimal interaction between the dressing material and the wound microenvironment (Figure 8, Tables 1 and 2).

The correspondence between structural tissue regeneration and surface-level healing emphasizes the critical role of dressing composition in guiding both the rate and quality of burn wound repair. These results underscore the importance of integrating histological evaluation into preclinical wound healing studies to fully understand treatment performance.

3.3.2. Evolution of Immunohistochemical Features in Burn Wounds

In the V group, TNF-α expression remained elevated, consistent with an active inflammatory phase, while VEGF activity suggested ongoing but comparatively slower angiogenesis. The persistence of necrotic tissue and reduced macrophage activity further indicated a delayed overall healing process in this group (Figure 9, Table 3).

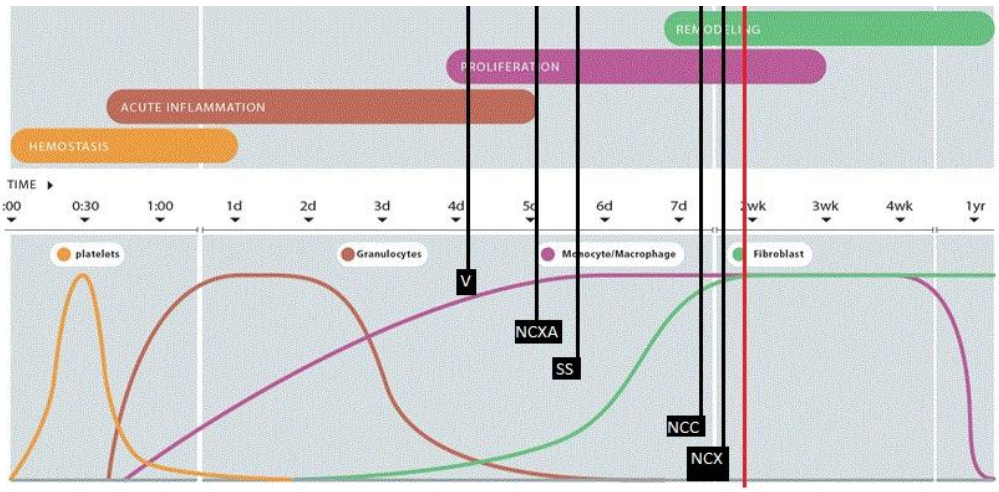

Figure 9. Healing progress of each study group at day 11, relative to the standard theoretical healing timeline (red line), according to relevant cell populations. The proliferative phase should be at a peak, with an equally important presence of fibroblast that triggers remodelling and wound contraction. NCC and NCX are evolving accordingly, while the natural healing is still in a highly inflammatory phase, confirming a deep dermal burn. NCXA and SS biopsies reveal increased inflammatory activity relative to the other groups.

 doi:10.20944/preprints202606.1266.v1

Rats treated with SS exhibited a similar immunohistochemical profile to the V group, except for VEGF levels, which reflected the advanced stage of angiogenesis. Reduced exudate and necrosis relative to V confirmed the superior efficacy of SS, with wound healing progressing according to expected patterns (Figure 9, Table 3).

NCC-treated wounds showed elevated inflammatory markers alongside well-developed functional neo vessels, indicating a favourable healing trajectory. In the NCX group (CS/TMC nanofibers loaded with norfloxacin), the inflammatory response was most pronounced at day 11, accompanied by active collagen deposition, established neovascularization, and a multilayered epidermis (Figure 9, Table 3).

In the NCXA group, the histological profile resembled that of the SS group, though with slightly increased superficial dermal inflammation. The lowest observed levels of cellular differentiation and neovascularization in this group suggested a comparatively slower healing rate (Figure 9, Table 3).

Table 3. IHC Markers expression at Day 11 (+++ is high, ++ is moderate, + is low).

IHC Marker	V	SS	NCXA	NCX	NCC
TNF-α	++	++	++	+++	+++
IL-1β	+++	+++	+++	++	+++
CD163	++	++	++	+++	++
IL-17	+	++	++	++	++
VEGF	+++	+	++	+	++
VCAM	+	+	+	+	++

In the NCXA group, the histological profile resembled that of the SS group, though with slightly increased superficial dermal inflammation. The lowest observed levels of cellular differentiation and neovascularization in this group suggested a comparatively slower healing rate (Figure 9, Table 3).

Persistent elevations of TNF-α, IL-1β, and CD163 in the V-treated wounds indicate ongoing acute inflammation, while sustained VEGF activity at three weeks suggests continued vascular remodelling and a potential shift toward a chronic inflammatory state despite complete epithelialization (Figures 10 and 11 and Table 4).

Table 4. IHC markers expression at Day 22 (+++ is high, ++ is moderate, + is low, 0 is mostly absent).

Marker IHC	V	SS	NCXA	NCX	NCC
TNF-α	+++	++	+	0	+
IL-1β	+++	++	+++	++	+++
CD163	+++	++	++	++	++
IL-17	+	++	+++	++	+++
VEGF	+++	+++	++	+	+++
VCAM	+	+	++	+	+++

Moderate generalized inflammation was observed with SS treatment, accompanied by well-preserved cellular differentiation, the highest degree of macroscopic wound contraction, and epidermal thickness and cellularity comparable to the Vaseline group, reflecting effective but not fully optimized tissue repair (Figure 10, Table 4).

Wounds treated with NCC nanofibers exhibited improved skin quality with multilayered epidermis and active collagen synthesis and resorption, indicative of ongoing robust healing (Figure 10, Table 4).

Complete epithelialization was achieved in wounds treated with NCX nanofibers, which also showed the lowest TNF-α, VEGF, and VCAM expression, minimal inflammatory profile, moderate CD163 and IL-17 levels reflecting keratinocyte proliferation and deep dermal regeneration, and fully established angiogenesis. Extensive tissue infiltration, necrotic debris, and pronounced dermal

 doi:10.20944/preprints202606.1266.v1

inflammation were evident in wounds treated with NCXA nanofibers, indicating present macrophage activity, thus a severely delayed healing process (Figure 10, Table 3).

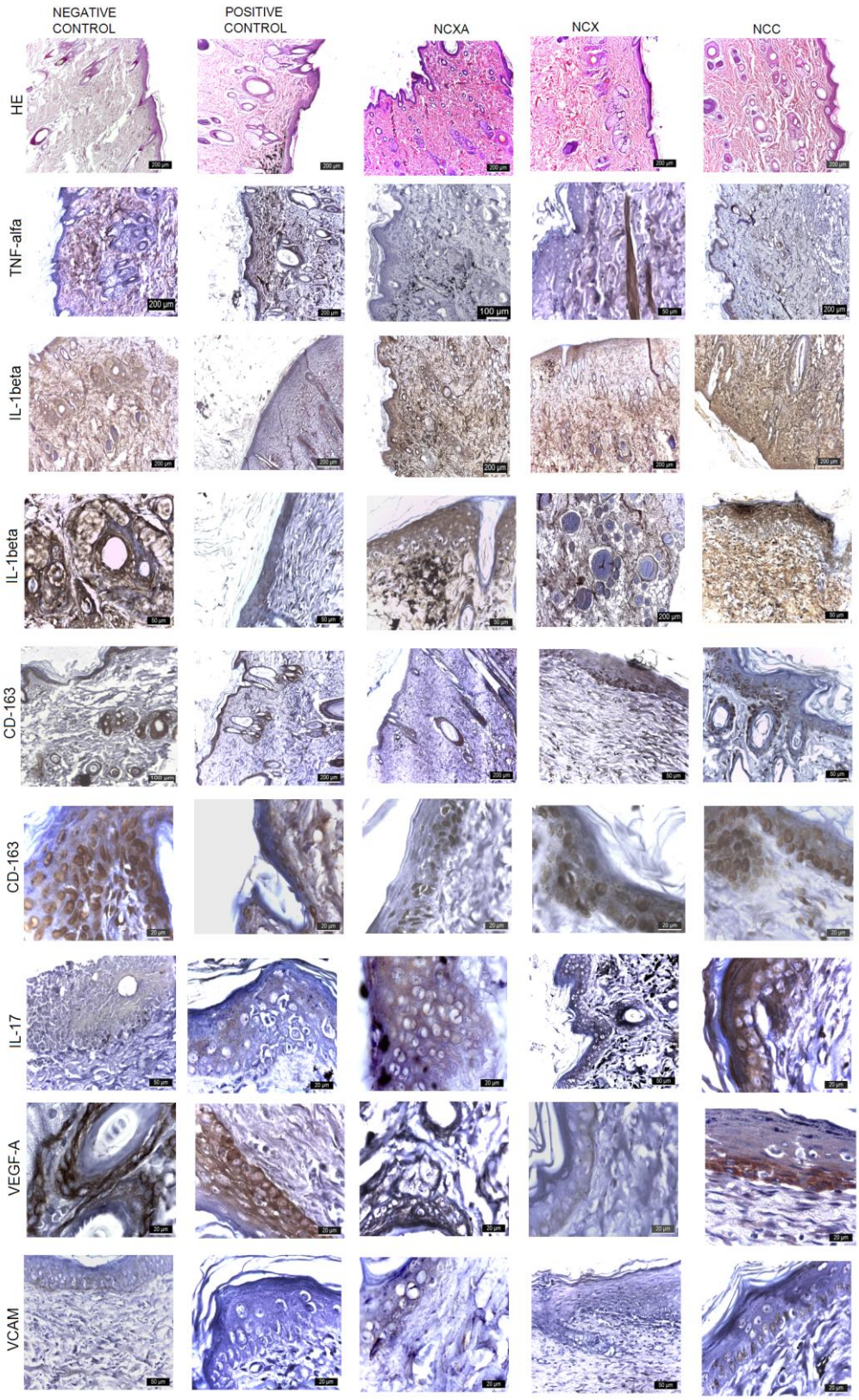

Figure 10. Immunohistochemical staining of the dressing tested at endpoint (day 22).

 doi:10.20944/preprints202606.1266.v1

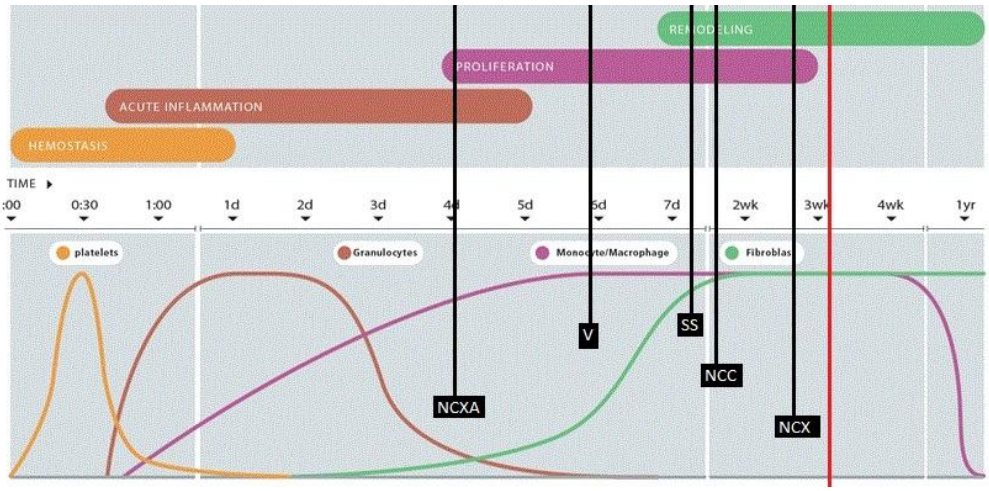

Figure 11. Healing progress of each study group at day 22, relative to the standard theoretical healing timeline (red line), according to relevant cell populations. The proliferative phase should already diminish the intensity, while the fibroblasts dominate. NCX is the only group that follows the natural healing curve of a 'simple' wound. The natural healing (V) is slowly advancing through a prolonged inflammatory phase, while SS and NCC show intermediate progress. NCXA is stagnating in a highly inflammatory phase, like a chronic wound.

3.3.4. Systemic Inflammation Impact

No significant differences were detected in standard haematological parameters, including red blood cell count (RBC), haemoglobin concentration (Hb), and haematocrit (Ht), across the experimental groups. Likewise, liver and kidney function markers remained within comparable ranges, indicating that the application of the topical dressings did not induce systemic toxicity or adversely affect major organ function (data not showed).

Interestingly, IL-8 was the only serum inflammatory marker to show a statistically significant difference among the groups. Interleukin-8 is a key chemokine involved in the recruitment and activation of neutrophils at sites of tissue injury, playing a central role in the early inflammatory phase of wound healing. Serum IL-8 levels were monitored at multiple time points to capture dynamic changes during the healing process, and the results are summarized in Figure 12. The observed differences in IL-8 suggest that the type of dressing can modulate the systemic inflammatory response, potentially reflecting variations in local wound microenvironment signalling and the progression from inflammation to tissue repair.

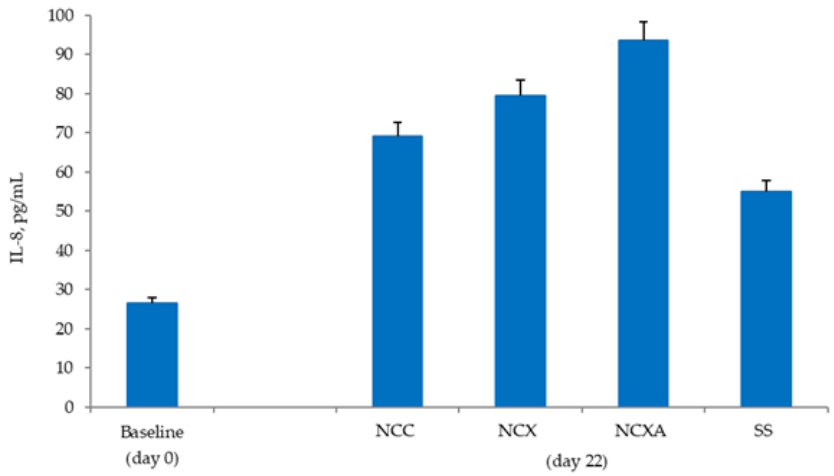

 doi:10.20944/preprints202606.1266.v1

Figure 12. The influence of the dressing used on the blood level of IL-8 in the experiment. The values are presented as mean ± standard deviation of mean (S.D.) for 5 rats per group.

These findings emphasize the importance of evaluating both systemic and local immunological responses in preclinical wound healing studies. While standard hematological and biochemical parameters confirm the safety of the tested materials, changes in specific inflammatory mediators like IL-8 provide insight into the interplay between topical interventions and host immune regulation during tissue regeneration.

4. Discussions

4.1. Overall Therapeutic Performance of Functionalized CS/TMC Nanofibers

Building on our previous work, which demonstrated that electrospinning CS and TMC in controlled ratios yields nanofibrous materials with tunable structural and biological properties [27,30,52–54], we explored strategies to further enhance their therapeutic potential in wound healing. Among the ratios tested, a predominance of CS by a factor of seven was identified as optimal for in vivo applications, providing a balance of mechanical stability, biocompatibility, and bioactivity.

In this study, two functionalization approaches were implemented to extend the activity spectrum of the fibers: NCX and NCXA. Pristine CS/TMC fibers were included as NCC to isolate the effects of drug incorporation and surface modification.

Morphological analyses confirmed that the nanofibrous architecture was largely preserved following both encapsulation and imination. Although minor crystalline aggregates of norfloxacin were occasionally observed, the drug was predominantly well-dispersed throughout the fiber matrix, ensuring uniform bioavailability. Structural characterization further validated the successful incorporation of all components without residual synthetic polymer, indicating that both functionalization strategies were effectively realized.

Functionally, all tested dressings demonstrated measurable wound-healing activity in the standardized second-degree burn model. Notably, the NCX-treated wounds exhibited complete closure by day 22, highlighting the role of localized antibiotic delivery in accelerating epithelialization and reducing microbial burden. Macroscopic evaluation, H&E staining, and immunohistochemistry collectively provided a multi-dimensional view of tissue regeneration, revealing that NCX fibers promoted not only faster closure but also organized dermal reconstruction and reduced inflammatory infiltration. The NCXA group showed enhanced antifungal potential, with histological markers indicating modulation of the inflammatory phase, although some residual ulcerations persisted, suggesting that combined loading and surface functionalization may influence the kinetics of tissue remodelling. Across all groups, the concordance between macroscopic and histological/IHC assessments reinforced the robustness of the findings [3,7,55].

Overall, these results illustrate that electrospun CS/TMC fibers can serve as versatile platforms for the controlled delivery of bioactive agents, with functionalization strategies directly influencing both the rate and quality of wound healing. This integrated, mechanistic perspective underscores the potential of these materials for tailored, multi-functional wound dressings in regenerative medicine.

Among the tested dressings, NCX emerged as the most effective in promoting both rapid wound closure and high-quality skin regeneration. By day 22, the inflammatory response had largely subsided, consistent with the remodelling phase of tissue repair. The low serum and tissue levels of TNF-α indicated the resolution of acute inflammation, while markers such as CD163 and IL-17, known to regulate macrophage polarization, cell differentiation, and extracellular matrix remodelling, were prominently expressed [45,47]. According to the designated scoring system, NCX consistently exhibited minimal activity in the inflammatory phase (yellow region of the chart), highlighting its ability to orchestrate a balanced transition from inflammation to proliferation and remodelling. These results collectively suggest that NCX not only accelerates epithelialization but also supports the formation of well-organized dermal structures and functional skin architecture.

 doi:10.20944/preprints202606.1266.v1

By contrast, NCXA displayed a markedly different healing trajectory. Although it initially triggered an inflammatory response comparable to other treatments at day 11, progression into the remodelling phase was delayed. Persistent elevations of TNF-α and IL-1β, alongside ongoing cellular debris, indicated that the acute inflammatory phase was prolonged, despite evidence of epidermal regeneration mediated by CD163 and IL-17 [56]. This suggests that the local chemical environment, potentially influenced by the boronic acid or by its concentration, contributed to delayed resolution rather than microbial infection, as neither bacterial nor fungal colonization was observed macroscopically or histologically. Importantly, systemic inflammatory markers remained unchanged in the NCXA group, indicating a localized effect.

Analysis of VEGF expression further supports this interpretation. In most groups, VEGF peaked at day 11, corresponding to the onset of the proliferative phase. In contrast, NCXA exhibited elevated VEGF levels at day 22, reflecting a delayed angiogenic response consistent with a prolonged early proliferative phase and ongoing tissue remodelling [57,58]. These findings suggest that NCXA modulates wound healing differently, likely prolonging the inflammatory phase while partially supporting epidermal regeneration, which collectively results in slower, less coordinated tissue repair.

Taken together, these results highlight the superiority of NCX in orchestrating a rapid, high-quality healing process by effectively balancing inflammation, proliferation, and remodelling. In contrast, NCXA's local chemical effects appear to sustain inflammation and delay maturation, illustrating how subtle differences in dressing composition can critically influence the kinetics and quality of wound repair.

The delayed healing observed in the NCXA-treated wounds may be attributed to the specific interactions between the dressing and the wound microenvironment. Elevated levels of VEGF and VCAM in this group indicate a delayed transition into the proliferative phase, occurring beyond two weeks, which is consistent with characteristics of a "chronic wound" phenotype [59–62], as illustrated in Figure 10.

The NCC and SS groups exhibited comparable healing dynamics, with H&E staining and immunohistochemical profiles showing similar expression patterns across all assessed markers. In contrast, wounds in the V group healed as expected for a second-degree burn, but with poorly formed epithelium and sustained inflammatory activity. Such burns are prone to excessive contraction and may progress toward keloid or hypertrophic scarring if left to remodel naturally.

Serum IL-8 levels reflected the complex interplay of multiple ongoing processes, including burn repair, collagen synthesis and reorganization, and acute responses triggered by the skin biopsy performed on day 11. Elevated IL-8 has been associated with enhanced wound healing, accelerated keratinocyte proliferation [63,64], and the transition from the inflammatory to the proliferative phase [65], whereas persistently low IL-8 levels often correlate with delayed or impaired healing [63]. Persistent elevation of IL-8 following burn injury is typical, although the precise temporal dynamics were not investigated in this study [66,67]. Given that IL-8 can also be elevated in systemic conditions such as sepsis, pulmonary distress, or acute injury, these results must be interpreted in the clinical and experimental context rather than in isolation [68,69].

4.2. Study Limitations and Methodological Considerations

Several limitations should be acknowledged when interpreting the present findings. The relatively small sample size (n = 5 per group), although consistent with preliminary in vivo screening studies, may limit statistical power; however, the consistency of trends observed across macroscopical, histological, and immunohistochemical evaluations supports the robustness of the main observations. The study design focused on comparing selected formulations within a controlled experimental framework and did not include other advanced wound dressings (e.g., hydrogels or alginates), which may limit direct benchmarking against the full spectrum of currently available materials.

 doi:10.20944/preprints202606.1266.v1

The rat burn model, while widely used and highly reproducible, presents known anatomical and physiological differences compared to human skin, including the presence of the panniculus carnosus and an enhanced intrinsic healing capacity; therefore, the results should be interpreted primarily as proof-of-concept rather than directly translatable outcomes.

The absence of infection in this model, due to controlled experimental conditions, did not allow a full in vivo assessment of antimicrobial performance, although the selected drug and materials have well-documented antibacterial activity in the literature. The selected evaluation time points (days 11 and 22) were chosen to capture representative stages of the proliferative and remodelling phases; however, intermediate time points could provide additional insight into early inflammatory dynamics.

Immunohistochemical assessment was conducted using a semi-quantitative scoring approach, which, while commonly employed in similar studies, may introduce observer-dependent variability; nonetheless, this was mitigated by the parallel use of multiple markers and complementary histological evaluation. Finally, the use of a standardized but customized experimental setup ensured reproducibility within the study, although replication in other laboratories may require adaptation of the protocol.

4.3. Implications for the Rational Design and Evaluation of Bioengineered Wound Dressings

Assessment of wound healing extends beyond the mere observation of epithelial closure, as rapid wound contraction does not necessarily equate to high-quality tissue regeneration or optimal scar formation. This study highlights the importance of a comprehensive, multi-level evaluation, incorporating macroscopic inspection, histological analysis, and IHC, to accurately interpret healing outcomes. By integrating these methodologies, we were able to identify molecular and cellular markers corresponding to distinct phases of wound repair, thereby distinguishing between effective tissue regeneration and prolonged inflammatory responses.

These findings carry significant implications for the design and evaluation of bioengineered wound dressings. They underscore that dressing performance should not be assessed solely based on closure rates but must also consider tissue quality, cellular differentiation, extracellular matrix organization, and vascular maturation. To our knowledge, this is the first study to apply such a holistic characterization to chitosan-based scaffolds, providing a robust framework for future preclinical and translational investigations in the field of regenerative wound care.

5. Conclusions

The present work demonstrated the successful fabrication and subsequent modification of trimethyl chitosan/chitosan nanofibrous systems, yielding both antibiotic-loaded and surface-engineered candidates for advanced wound management. Structural and chemical analyses verified the achievement of homogeneous fibrous architectures, effective encapsulation of norfloxacin, and the successful introduction of functional groups via Schiff base formation.

In vivo testing using a rat burn model indicated that all investigated chitosan-derived materials contributed positively to tissue repair when compared with the untreated control group. The formulation incorporating norfloxacin alone exhibited the most efficient therapeutic response, reflected by faster re-epithelialization, a marked decrease in late-stage inflammatory signals, and more organized tissue reconstruction. Conversely, the additional chemical modification with 2-formylphenylboronic acid appeared to impair the healing trajectory, being associated with prolonged inflammatory activity and a slower transition into the remodelling phase, which points to the need for further refinement of both composition and loading strategy.

Integrated histological, immunohistochemical, and systemic assessments emphasize that subtle variations in formulation architecture can significantly influence the equilibrium between inflammatory resolution and regenerative processes. Overall, the results underline the promise of norfloxacin-loaded trimethyl chitosan nanofibers as multifunctional platforms for localized, controlled drug delivery in wound care applications.

 doi:10.20944/preprints202606.1266.v1

This investigation offers a conceptual basis for the further rational engineering of chitosan-based nanostructured systems aimed at optimized wound healing performance, while also indicating the necessity of additional studies to improve biological outcomes and support future translational development.

Author Contributions: Conceptualization, C.-G.C., I.G. and L.M.T.; methodology, C.-G.C., I.G., and C.S.; software, C.G.T., and C.C.; validation, I.G., and L.M.T.; formal analysis, C.G.T., C.C. and G.D.; investigation, C.-G.C., I.G., C.S., C.C., and G.D.; resources, C.-G.C., C.S. and L.M.T.; data curation, C.S., C.G.T., and G.D.; writing—original draft preparation, C.-G.C., C.G.T., C.C., G.D.; writing—review and editing, I.G., C.S., and L.M.T.; visualization, C.G.T., C.C. and G.D.; supervision, I.G. and L.M.T.; project administration, C.-G.C. and L.M.T.; funding acquisition, C.-G.C. All authors have read and agreed to the published version of the manuscript.

Funding: This research was supported by the Ministry of Research, Innovation and Digitization, CNCS/CCCDI–UEFISCDI, through project no. 538PED/2020 and project no. PCE 2/2021 within PNCDI III. Additional support was provided by the European Commission through the H2020-MSCA-RISE-2019 project SWORD-DLV-873123. The APC was funded by the authors.

Institutional Review Board Statement: The animal study protocol was approved by the Institutional Review Board (or Ethics Committee) of "Grigore T. Popa" University of Medicine and Pharmacy, Iași (Certificate No. 160/04.03.2022 and Project Authorization No. 56/19.02.2022, approved on 19.02.2022). The study was conducted in strict accordance with applicable national and international ethical guidelines for the care and use of laboratory animals, including the principles of the European Directive 2010/63/EU and Romanian Law No. 43/2014, ensuring the welfare and humane treatment of all animals throughout the study.

Data Availability Statement: The data supporting the findings of this study are available from the corresponding author upon reasonable request.

Acknowledgments: The authors would like to thank all collaborators and technical staff from CEMEX for their assistance with the experimental procedures. Special thanks are also extended to Bianca Andreica, Alexandru Anisiei, and Sandu Cibotaru from the Petru Poni Institute of Macromolecular Chemistry, Iași, for their essential contribution to the synthesis and physicochemical characterization of the nanofibrous materials employed in this study.

Conflicts of Interest: The authors declare no conflicts of interest.

References

1. Greaves, Ian.; Porter, K.M.; Garner, Jeff. *Trauma Care Manual*; Hodder Arnold, **2009**; ISBN 0340928263.
2. Foster, K.N.; Caruso, D.M. *Burn Resuscitation*; Elsevier Health Sciences, **2016**; ISBN 9780323463058.
3. Żwierełło, W.; Piorun, K.; Skórka-Majewicz, M.; Maruszewska, A.; Antoniewski, J.; Gutowska, I. Burns: classification, pathophysiology, and treatment: A Review. *Int. J. Mol. Sci*. **2023**, *24*, doi:10.3390/IJMS24043749.
4. Ahmad, N. In vitro and in vivo characterization methods for evaluation of modern wound dressings. *Pharmaceutics* **2023**, *15*, doi:10.3390/PHARMACEUTICS15010042.
5. Rashdan, H.R.M.; El-Naggar, M.E. Traditional and modern wound dressings—characteristics of ideal wound dressings. *Antimicrobial Dressings: The Wound Care Applications* **2023**, *21–42*, doi:10.1016/B978-0-323-95074-9.00002-6.
6. Janahmadi, Z.; Motlagh, M.R.; Zaeri, S. Enhancing rat full-thickness skin wounds with a mixed aloe/chitosan gel. *Formos. J. Surg.* **2019**, *52*, 84–91, doi:10.4103/FJS.FJS_109_18.
7. Gardikiotis, I.; Cojocaru, F.D.; Mihai, C.T.; Balan, V.; Dodi, G. Borrowing the features of biopolymers for emerging wound healing dressings: a review. *Int. J. Mol. Sci.* **2022**, *23*, doi:10.3390/ijms23158778.
8. Gounden, V.; Singh, M. Hydrogels and wound healing: current and future prospects. *Gels* **2024**, *10*, doi:10.3390/gels10010043.

 doi:10.20944/preprints202606.1266.v1

9. Haghighi, Z.; Asadi, M. The effects of chitosan-based nanofibers /peo/ henna extract on recovery of superficial second-degree burn in rat. *MBTJ* **2019**, *3*, 26–28, doi:10.22034/mbt.2019.80840.
10. Honardar, S.; Kordestani, S.S.; Daliri, M.; NayebHabib, F. The effect of chitosan-based gel on second degree burn wounds. *J. Wound Care* **2016**, *25*, 488–494, doi:10.12968/JOWC.2016.25.8.488.
11. Joshi, A.P.; Saad, M.; Mohan, M. A Review on burn and burn models in animals. *J. Basic Pharmacol. Toxicol.* **2017**, *1*, 1–8.
12. Kearns, R.D.; Holmes, J.H.; Cairns, B.A. Burn Injury: What's in a name? labels used for burn injury classification: a review of the data from 2000-2012. *Ann. Burns Fire Disasters* **2013**, *26*, 115–120.
13. Andreica, B.I.; Cheng, X.; Marin, L. Quaternary ammonium salts of chitosan. a critical overview on the synthesis and properties generated by quaternization. *Eur. Polym. J.* **2020**, *139*, 110016, doi:10.1016/j.eurpolymj.2020.110016.
14. Nagy, V.; Quader, S.; Másson, M. Fine-tuning the cytotoxicity profile of N,N,N-trimethyl chitosan through trimethylation, molecular weight, and polyelectrolyte complex nanoparticles. *Int. J. Biol. Macromol.* **2024**, *281*, doi:10.1016/j.ijbiomac.2024.135805.
15. Tabriz, A.; Ur Rehman Alvi, M.A.; Khan Niazi, M.B.; Batool, M.; Bhatti, M.F.; Khan, A.L.; Khan, A.U.; Jamil, T.; Ahmad, N.M. Quaternized trimethyl functionalized chitosan based antifungal membranes for drinking water treatment. *Carbohydr. Polym.* **2019**, *207*, 17–25, doi:10.1016/j.carbpol.2018.11.066.
16. Kirichenko, A.K.; Bolshakov, I.N.; Ali-Rizal, A.E.; Vlasov, A.A. Morphological study of burn wound healing with the use of collagen-chitosan wound dressing. bull. *Exp. Biol. Med.* **2013**, *154*, 692–696, doi:10.1007/S10517-013-2031-6.
17. Massand, S.; Cheema, F.; Brown, S.; Davis, W.J.; Burkey, B.; Glat, P.M. The use of a chitosan dressing with silver in the management of paediatric burn wounds: a pilot study. *J. Wound Care* **2017**, *26*, S26–S30, doi:10.12968/jowc.2017.26.Sup4.S26.
18. Kong, M.; Chen, X.G.; Xing, K.; Park, H.J. Antimicrobial properties of chitosan and mode of action: a state of the art review. *Int. J. Food Microbiol.* **2010**, *144*, 51–63, doi:10.1016/J.IJFOODMICRO.2010.09.012.
19. Li, P.; Poon, Y.F.; Li, W.; Zhu, H.Y.; Yeap, S.H.; Cao, Y.; Qi, X.; Zhou, C.; Lamrani, M.; Beuerman, R.W.; et al. A polycationic antimicrobial and biocompatible hydrogel with microbe membrane suctioning ability. *Nat. Mater.* **2011**, *10*, 149–156, doi:10.1038/NMAT2915.
20. Ahsan, S.M.; Thomas, M.; Reddy, K.K.; Sooraparaju, S.G.; Asthana, A.; Bhatnagar, I. Chitosan as biomaterial in drug delivery and tissue engineering. *Int. J. Biol. Macromol.* **2018**, *110*, 97–109, doi:10.1016/J.IJBIOMAC.2017.08.140.
21. Metcalfe, A.D.; Ferguson, M.W.J. Tissue engineering of replacement skin: the crossroads of biomaterials, wound healing, embryonic development, stem cells and regeneration. *J. R. Soc. Interface* **2007**, *4*, 413, doi:10.1098/RSIF.2006.0179.
22. Boateng, J.; Catanzano, O. Advanced therapeutic dressings for effective wound healing-a review. *J. Pharm. Sci.* **2015**, *104*, 3653–3680, doi:10.1002/JPS.24610.
23. Radzikowska-Büchner, E.; Łopuszyńska, I.; Flieger, W.; Tobiasz, M.; Maciejewski, R.; Flieger, J. An overview of recent developments in the management of burn injuries. *IJMS* **2023**, *24*: 24, 16357, doi:10.3390/IJMS242216357.
24. Marin, L.; Andreica, B.I.; Anisiei, A.; Cibotaru, S.; Bardosova, M.; Materon, E.M.; Oliveira, O.N. Quaternized chitosan (nano)fibers: a journey from preparation to high performance applications. *Int. J. Biol. Macromol.* **2023,** *242*, doi:10.1016/J.IJBIOMAC.2023.125136.
25. Abbaszadeh, A.; Rajabzadeh, A.; Zarei, L. Effect of chitosan/propolis biodegradable film on full-thickness wound healing in rats. *Iran. J. Vet. Surg.* **2019**, *14*, 9–17, doi:10.22034/IVSA.2019.159383.1168.
26. Matica, M.A.; Aachmann, F.L.; Tøndervik, A.; Sletta, H.; Ostafe, V. Chitosan as a wound dressing starting material: antimicrobial properties and mode of action. *Int. J. Mol. Sci.* **2019**, *20*, doi:10.3390/ijms20235889.
27. Anisiei, A.; Andreica, B.I.; Mititelu-Tartau, L.; Coman, C.G.; Bilyy, R.; Bila, G.; Rosca, I.; Sandu, A.I.; Amler, E.; Marin, L. Biodegradable trimethyl chitosan nanofiber mats by electrospinning as bioabsorbable dressings for wound closure and healing. *Int. J. Biol. Macromol.* **2023**, *249*, 126056, doi:10.1016/J.IJBIOMAC.2023.126056.

 doi:10.20944/preprints202606.1266.v1

28. Cibotaru, S.; Anisiei, A.; Platon, V.M.; Rosca, I.; Sandu, I.A.; Coman, C.G.; Mititelu-Tartau, L.; Andreica, B.I.; Marin, L. Imino-quaternized chitosan/chitosan nanofibers loaded with norfloxacin as potential bandages for wound healing. *Int. J. Biol. Macromol.* **2025**, *314*, doi:10.1016/j.ijbiomac.2025.144304.
29. Martinová, L.; Lubasová, D. Electrospun chitosan based nanofibers. *Res J Text Appar* **2008**, *12*, 72–79, doi:10.1108/RJTA-12-02-2008-B009.
30. Anisiei, A.; Rosca, I.; Sandu, A.I.; Bele, A.; Cheng, X.; Marin, L. Imination of microporous chitosan fibers—a route to biomaterials with "on demand" antimicrobial activity and biodegradation for wound dressings. *Pharmaceutics* **2022**, *14*, doi:10.3390/PHARMACEUTICS14010117/S1.
31. Borys, K.M.; Wieczorek, D.; Pecura, K.; Lipok, J.; Adamczyk-Woźniak, A. Antifungal activity and tautomeric cyclization equilibria of formylphenylboronic acids. *Bioorg. Chem.* **2019**, *91*, doi:10.1016/j.bioorg.2019.103081.
32. Silverman, Jerald.; Suckow, M.A.; Murthy, Sreekant.; National Institutes of Health (U.S.). *Institutional Animal Care and Use Committee. The IACUC Handbook*; CRC Press, **2007**; ISBN 9780849340109.
33. Cai, E.Z.; Ang, C.H.; Raju, A.; Tan, K.B.; Hing, E.C.H.; Loo, Y.; Wong, Y.C.; Lee, H.; Lim, J.; Moochhala, S.M.; et al. Creation of consistent burn wounds: a rat model. *Arch. Plast. Surg.* **2014**, *41*, 317–324, doi:10.5999/aps.2014.41.4.317.
34. Mitsunaga Junior, J.K.; Gragnani, A.; Ramos, M.L.C.; Ferreira, L.M. Rat an experimental model for burns: a systematic review. *Acta Cir. Bras.* **2012**, *27*, 417–423, doi:10.1590/S0102-86502012000600010.
35. IACUC UIOWA Available online: https://animal.research.uiowa.edu/iacuc-guidelines-anesthesia (accessed on 8 July 2024).
36. G.N.; G.R.-C.; M.S.; C.C.-G.; M.Ş.; N.M.M.; N.G.-V.; S.T.-T.; P.D. device for inducing skin burns in experimental animal models, using hot vapour, in a controlled manner. Osim ROMANIA **2016**.
37. Gouma, E.; Simos, Y.; Verginadis, I.; Lykoudis, E.; Evangelou, A.; Karkabounas, S. A simple procedure for estimation of total body surface area and determination of a new value of meeh's constant in rats. *Lab. Anim.* **2012**, *46*, 40–45, doi:10.1258/la.2011.011021.
38. Tatarusanu, S.M.; Lupascu, F.G.; Profire, B.S.; Szilagyi, A.; Gardikiotis, I.; Iacob, A.T.; Caluian, I.; Herciu, L.; Giscă, T.C.; Baican, M.C.; et al. Modern approaches in wounds management. *Polymers (Basel).* **2023**, *15*, doi:10.3390/polym15173648.
39. Iacob, A.T.; Drăgan, M.; Gheţu, N.; Pieptu, D.; Vasile, C.; Buron, F.; Routier, S.; Giusca, S.E.; Caruntu, I.D.; Profire, L. Preparation, characterization and wound healing effects of new membranes based on chitosan, hyaluronic acid and arginine derivatives. *Polymers (Basel).* **2018**, *10*, doi:10.3390/POLYM10060607.
40. Sánchez-Machado, D.I.; López-Cervantes, J.; Martínez-Ibarra, D.M.; Escárcega-Galaz, A.A.; Vega-Cázarez, C.A. The use of chitosan as a skin-regeneration agent in burns injuries: a review. *E-Polymers* **2022**, *22*, 75–86, doi:10.1515/EPOLY-2022-0011/ASSET/GRAPHIC/J_EPOLY-2022-0011_FIG_002.JPG.
41. Tavares Pereira, D.D.S.; Lima-Ribeiro, M.H.M.; De Pontes-Filho, N.T.; Carneiro-Leão, A.M.D.A.; Correia, M.T.D.S. Development of animal model for studying deep second-degree thermal burns. *J. Biomed. Biotechnol.* **2012**, *2012*, doi:10.1155/2012/460841.
42. Ghetu N, C.C. *Device for Quick Fixing, Retaining and Protecting Bandage to Be Used in Small Laboratory Animals* **2016**.
43. Heimann, M.; Käsermann, H.P.; Pfister, R.; Roth, D.R.; Bürki, K. Blood collection from the sublingual vein in mice and hamsters: a suitable alternative to retrobulbar technique that provides large volumes and minimizes tissue damage. *Lab. Anim.* **2009**, *43*, 255–260, doi:10.1258/LA.2008.007073.
44. Fenner, J.; Clark, R.A.F. *Anatomy, physiology, histology, and immunohistochemistry of human skin*; Elsevier Inc., **2016**; ISBN 9780128016541.
45. Ferreira, D.W.; Ulecia-Morón, C.; Alvarado-Vázquez, P.A.; Cunnane, K.; Moracho-Vilriales, C.; Grosick, R.L.; Cunha, T.M.; Romero-Sandoval, E.A. CD163 overexpression using a macrophage-directed gene therapy approach improves wound healing in ex vivo and in vivo human skin models. *Immunobiology* **2020**, *225*, 151862, doi:10.1016/J.IMBIO.2019.10.011.
46. Krzyszczyk, P.; Schloss, R.; Palmer, A.; Berthiaume, F. The role of macrophages in acute and chronic wound healing and interventions to promote pro-wound healing phenotypes. *Front. Physiol.* **2018**, *9*, 419, doi:10.3389/FPHYS.2018.00419.

 doi:10.20944/preprints202606.1266.v1

47. Bechara, R.; McGeachy, M.J.; Gaffen, S.L. The metabolism-modulating activity of IL-17 signaling in health and disease. *J. Exp. Med.* **2021**, *218*, doi:10.1084/JEM.20202191.
48. Țiburcă, L.; Bembea, M.; Zaha, D.C.; Jurca, A.D.; Vesa, C.M.; Rațiu, I.A.; Jurca, C.M. The treatment with interleukin 17 inhibitors and immune-mediated inflammatory diseases. *Curr. Issues Mol. Biol.* **2022**, *44*, 1851, doi:10.3390/CIMB44050127.
49. Koh, T.J.; DiPietro, L.A. Inflammation and wound healing: the role of the macrophage. *Expert Rev. Mol. Med.* **2011**, 13, doi:10.1017/S1462399411001943.
50. Ailincai, D.; Cibotaru, S.; Anisiei, A.; Coman, C.G.; Pasca, A.S.; Rosca, I.; Sandu, A.I.; Mititelu-Tartau, L.; Marin, L. Mesoporous chitosan nanofibers loaded with norfloxacin and coated with phenylboronic acid perform as bioabsorbable active dressings to accelerate the healing of burn wounds. *Carbohydr. Polym.* **2023**, *318*, doi:10.1016/J.CARBPOL.2023.121135.
51. Ailincai, D.; Marin, L.; Morariu, S.; Mares, M.; Bostanaru, A.C.; Pinteala, M.; Simionescu, B.C.; Barboiu, M. Dual crosslinked iminoboronate-chitosan hydrogels with strong antifungal activity against candida planktonic yeasts and biofilms. *Carbohydr. Polym.* **2016**, *152*, 306–316, doi:10.1016/j.carbpol.2016.07.007.
52. Chanda, A.; Adhikari, J.; Ghosh, A.; Chowdhury, S.R.; Thomas, S.; Datta, P.; Saha, P. Electrospun chitosan/polycaprolactone-hyaluronic acid bilayered scaffold for potential wound healing applications. *Int. J. Biol. Macromol.* **2018**, *116*, 774–785, doi:10.1016/J.IJBIOMAC.2018.05.099.
53. RO138211A2 - Electrospinning process for chitosan nanofibers and quaternized chitosan/chitosan nanofibers - Google Patents Available online: https://patents.google.com/patent/RO138211A2/en?q=(anisiei)&inventor=marin&oq=marin+anisiei (accessed on 8 July **2024**).
54. Bejan, A.; Anisiei, A.; Andreica, B.I.; Rosca, I.; Marin, L. Chitosan nanofibers encapsulating copper oxide nanoparticles: a new approach towards multifunctional ecological membranes with high antimicrobial and antioxidant efficiency. *Int. J. Biol. Macromol.* **2024**, *260*, 129377, doi:10.1016/J.IJBIOMAC.2024.129377.
55. Banerjee, J.; Seetharaman, S.; Wrice, N.L.; Christy, R.J.; Natesan, S. Delivery of silver sulfadiazine and adipose derived stem cells using fibrin hydrogel improves infected burn wound regeneration. *PLoS One* **2019**, *14*, doi:10.1371/journal.pone.0217965.
56. Parrish, W.R. Physiology of blood components in wound healing: an appreciation of cellular co-operativity in platelet rich plasma action. *J. Exerc. Sports Orthop.* **2017**, *4*, 1–14, doi:10.15226/2374-6904/4/2/00156.
57. Grambow, E.; Sorg, H.; Sorg, C.G.G.; Strüder, D. Experimental models to study skin wound healing with a focus on angiogenesis. *Med Sci* **2021**, *9*: 55. doi:10.3390/MEDSCI9030055.
58. Vidinsk¯, B.; Gál, P.; Toporcer, T.; Longauer, F.; Lenhardt, A; Bobrov, N.; Sabo, J. Histological study of the first seven days of skin wound healing in rats. *Acta Vet. Brno* **2006**, *75*: 197-202.
59. Ellis, S.; Lin, E.J.; Tartar, D. Immunology of wound healing. *Curr. Dermatol. Rep.* **2018**, *7*, 350–358, doi:10.1007/S13671-018-0234-9/FIGURES/2.
60. Mu, X.; Gu, R.; Tang, M.; Wu, X.; He, W.; Nie, X. IL-17 in wound repair: bridging acute and chronic responses. *Cell Commun Signal* **2024**, *22*, doi:10.1186/S12964-024-01668-W.
61. Masson-Meyers, D.S.; Andrade, T.A.M.; Caetano, G.F.; Guimaraes, F.R.; Leite, M.N.; Leite, S.N.; Frade, M.A.C. Experimental models and methods for cutaneous wound healing assessment. *Int. J. Exp. Pathol.* **2020**, *101*, 21–37, doi:10.1111/IEP.12346.
62. Hesketh, M.; Sahin, K.B.; West, Z.E.; Murray, R.Z. Macrophage phenotypes regulate scar formation and chronic wound healing. *Int. J. Mol. Sci.* **2017**, *18*, doi:10.3390/IJMS18071545.
63. Jiang, W.G., Sanders, A.J., Ruge, F., Harding, K.G. Influence of interleukin-8 (IL-8) and IL-8 receptors on the migration of human keratinocytes, the role of PLC-γ and potential clinical implications. *Exp Ther Med* **2012**, *3*: 231-236. https://doi.org/10.3892/etm.2011.402.
64. Rennekampff, H.O.; Hansbrough, J.F.; Kiessig, V.; Doré, C.; Sticherling, M.; Schröder, J.M. Bioactive interleukin-8 is expressed in wounds and enhances wound healing. *J. Surg. Res.* **2000**, *93*, 41–54, doi:10.1006/JSRE.2000.5892.
65. Piipponen, M.; Li, D.; Landén, N.X. The immune functions of keratinocytes in skin wound healing. *IJMS* **2020**, *21*: 8790, doi:10.3390/IJMS21228790.

 doi:10.20944/preprints202606.1266.v1

66. Korkmaz, H.I.; Flokstra, G.; Waasdorp, M.; Pijpe, A.; Papendorp, S.G.; de Jong, E.; Rustemeyer, T.; Gibbs, S.; van Zuijlen, P.P.M. The complexity of the post-burn immune response: an overview of the associated local and systemic complications. *Cells* **2023**, *12*: 345 doi:10.3390/CELLS12030345.
67. Finnerty, C.C.; Jeschke, M.G.; Branski, L.K.; Barret, J.P.; Dziewulski, P.; Herndon, D.N. Hypertrophic scarring: the greatest unmet challenge after burn injury. *The Lancet* **2016**, *388*, 1427–1436, doi:10.1016/S0140-6736(16)31406-4.
68. Al-Ani, F.W.; Fahad, H.M. Detection of the level of interleukin-8 in the serum of burn patients by ELISA technique. *Arch. Razi Inst.* **2023**, *78*, 1087, doi:10.22092/ARI.2022.359993.2529.
69. Yeh, F.L.; Lin, W.L.; Shen, H.D.; Fang, R.H. Changes in levels of serum IL-8 in burned patients. *Burns* **1997**, *23*, 555–559, doi:10.1016/S0305-4179(97)00071-5.